PHOTOCATALYTIC PERFORMANCE OF SYSTEMS BASED ON URANYL-INCORPORATED SBA-15 MESOPOROUS SILICA

D. D. DUMITRASCU[a], E. POPOVICI[b], N. VRINCEANU[a*], D. HUMELNICU[b], N. OUERFELLI[c], R. I. PREPELITA[d], I. GRADINARU[e]
[a]*"L.Blaga" University of Sibiu, 2-4 Ion Ratiu Street, 500204, Sibiu, Romania*
[b]*"Al. I. Cuza" University of Iasi, Bvd. Carol I, no 11, 700506, Romania*
[c]*Laboratoire de Technologies Médicales et Biophysique, Institut Supérieur des Technologies Médicales de Tunis, 9, Av. Dr. Zouhaier Essafi 1006 Tunis, Tunisia University of Tunis El Manar*
[d] *Gr.T. Popa" University of Medicine and Pharmacy of Iaşi, Faculty of Medicine, Department of Psychiatry, 16 Universitatii Street, 700115, Iasi, Romania*
[e]*"Gr. T. Popa" University of Medicine and Pharmacy of Iasi, Faculty of Dental Medicine, Department of Odontology, Periodontology, and Fixed Prosthodontics, 6 University Street, 700115 Iasi, Romania*

The present study investigated incorporating uranyl ions into solid porous matrices for long-term storage and, at the same time, the possibility of using excited uranyl ions as a photocatalyst for the degradation of dangerous pollutant molecules that may be ingested or inhaled. As a porous matrix, SBA-15 silica was used. The matrix synthesis consisted in a self-assembly process. The triblock copolymer Pluronic 123(EO20PO70EO20) was used as a template, under acidic conditions. Tetraethoxyorthosilicate played the role of silica source. The uranyl ions were heterogenized onto the large ordered pores of SBA-15 mesoporous silica. These pores served as ideal hosts for the encapsulation of uranyl species due to their high surface area, large pore size and high thermal stability. The samples were characterized by X-ray diffraction (XRD), Fourier transform infrared spectroscopy (FT-IR), diffuse reflectance ultraviolet–visible spectroscopy (DRUV–VIS), and nitrogen adsorption/desorption technique at 77K. The uranyl ions incorporated within the mesopores of silica host matrices served as highly efficient heterogeneous photocatalysts for room-temperature photooxidation of Eosin Y as a reactant in the photocatalytic batch reactor. The results indicate the potential applicability of uranyl encapsulated onto the SBA-15 silica photocatalyst in applications related to wastewater processing under ambient conditions.

(Received February 17, 2016; Accepted April 13, 2016)

Keywords: uranyl ions, SBA-15, photocatalysis, mesoporous silica, photocatalytically active species, mesoporous silica matrix

1. Introduction

Uranium is the most important element for the nuclear industry. It has a long half-life and a coordination chemistry consisting of multiple stable oxidation states and stable solid and aqueous forms within the ecosphere. Among the five oxidation states of uranium, only +4 and +6 are stable for practical considerations [1]. Under standard aqueous environmental conditions, uranium generally occurs in its hexavalent form, as does the uranyl ion, UO_2^{2+} [2]. The occurrence of uranium in soil, rocks, and groundwater is a serious problem for the environment because of its toxicity and radioactivity. On the basis of aquatic and terrestrial ecotoxicity data, a maximum permissible addition to background levels of 1.0 μg U per L in seawater, freshwater and groundwater has been suggested. When it comes to soil, a background concentration of 2.9 mg/kg has been determined and a maximum permissible concentration of 28.3 mg U/kg of soil has been

* Corresponding author: vrinceanu.narcisai@ulbsibiu.ro

suggested. On these grounds, the ion selective retention of uranium (VI) by various components of solid matter remains a subject of continuous efforts aimed at solving the issues of environmental clean-up. In this context, there is currently considerable interest in the incorporation of uranyl ions into solid matrices, such as activated carbon, metal oxides, as well as onto natural substrates. Modified microporous adsorbents have also been subject to many investigations [3,4]. Having as main objective the sorption of UO_2^{2+} derived from an aqueous solution ions of uranyl salt, some adsorbents such as zeolites, montmorillonite clays [5,6] silica gels [7], diatomite [8], and hydrous oxides [9] have been employed. Nevertheless, some disadvantages like inaccessible pores, or their small and irregular sizes, poor selectivity, low surface area, low capacity restricted their use to aim for these toxic metal ions [10]. On the other hand, the discovery of mesoporous silicas such as the M41S family has provided new opportunities in environmental and industrial processes [11, 12, 13, 14, 15]. Periodic mesoporous materials are extensively employed with a view to aiding in the dispersion of photocatalytically active species, since they possess very high surface areas, large pore volumes, and can be easily synthesized. They have remarkable features such as tunable structural and morphological properties, a large surface area (1000–1400 m^2/g) and uniform pores with well-defined and controlled sizes (2–10 nm). In an earlier study, reported on the adsorption of UO_2^{2+} ions on surfactant-free (calcined) mesoporous titanium-based materials [16]. These materials were shown to have a high capacity for UO_2^{2+} loading compared to the corresponding microporous material. Many other publications have illustrated different methods for anchoring uranyl ions within the silicate matrix of mesoporous MCM-41 and MCM-48 hosts [17,18,19]. Generally, the anchoring of uranyl ions onto porous matrices has been carried out by a number of methods, including direct template exchange inside structural channels using UO_2^{2+} ions in an aqueous solution, hydrothermal synthesis, impregnation/loading, and physical mixtures. Photochemical studies on uranium (VI) date back to the beginning of the 20^{th} century when uranyl oxalate was found to decompose under the influence of light [20, 21]. Uranyl ions are known to possess distinctive photoabsorption, excitation, and emission characteristics, as compared to other inorganic cations [21]. The lowest excited Eigen value of the uranyl ion (UO_2^{2+}) is a strongly oxidizing species (E = 2.6 V), which can be quenched by a variety of organic substrates, resulting in the abstraction of their hydrogen atoms [22, 23]. Some studies have been devoted to the photocatalytic activity of UO_2^{2+} ions in heterogeneous reaction mode. Suib and co-workers [24, 25, 15] employed uranyl-exchanged clays and zeolites for the photooxidation of ethanol, isopropyl alcohol, and diethyl ether to yield the corresponding aldehydes and ketones. These studies demonstrated that the restricted pore dimensions of zeolites and pillared clays may help in controlled product selectivity. Vidya et al. reported for the first time that uranyl ions anchored within the mesopores of MCM-41 may serve as an efficient heterogeneous photocatalyst for the complete destruction of methanol in the vapor phase, in the presence of sunlight and air [14, 26]. Uranyl-anchored MCM-41 was found to be more efficient than a TiO_2 photocatalyst in terms of CH_3OH to CO_2 conversion rates. To our knowledge, the use of SBA-15 mesoporous silica as a uranyl ion loading matrix or photocatalytic system under UV and sunlight conditions has not yet been reported. SBA-15 is a mesoporous silica sieve possessing uniform hexagonal pores with a narrow pore size distribution and a tunable pore diameter of between 5 and 15 nm.

The present original laboratory-scale study fits into a currently active field with the aim of incorporating uranyl ions into solid porous matrices for long-term storage. At the same time, excited uranyl ions may potentially be used as a photocatalyst for the degradation of Eosin Y dye.

2. Experimental

2.1. SBA-15 mesoporous synthesis (support - sample S)

The matrix of SBA-15 was synthesized by a cooperative self-assembly process under acidic conditions using the triblock copolymer Pluronic 123 ($EO_{20}PO_{70}EO_{20}$) as a template with tetraethoxyorthosilicate (TEOS, Sigma-Aldrich) as the silica source. The silica SBA-15 support was synthesized by the hydrothermal method using the method reported by Zhao and Vidya [26, 17]. In a typical synthesis procedure, the triblock copolymer Pluronic P123 ($EO_{20}PO_{70}EO_{20}$, Aldrich) was dissolved in a mixture of water and 37% HCl. The mixture was stirred and then

heated in an oil bath to 45°C, then TEOS was added, and a mixture with the molar composition TEOS:5.87 HCl:194 H_2O:0.017 P123 was obtained. The resulting synthesis mixture was stirred at 45°C for 7.5 h, and then heated at 80°C under static conditions for 15 h. The as-synthesized SBA-15 silica was recovered by filtration, washed with distilled water, dried and calcined in a flow of air, at 550°C for 6 h (1°C min^{-1}).

2.2. Incorporation of uranyl in the SBA-15 matrix

The incorporation of uranyl ions was carried out through various methods such as: (A) hydrothermal synthesis (sample H), (B) direct template exchange inside mesoporous channels by UO_2^{2+} ions in an aqueous solution (sample D), and (C) impregnation/loading (sample I).

Hydrothermal synthesis of uranyl-incorporated SBA-15 (sample H)

In what can be described as a typical synthesis procedure, the triblock copolymer Pluronic 123 was dissolved in a mixture of 0.005 M uranyl nitrate [$UO_2(NO_3)_2$, Sigma] and HNO_3 solution, followed by stirring and then heating in an oil bath to 45°C; TEOS was then added, and the mixture of molar composition TEOS:5.8 HNO_3:194 H_2O:0.017 P123:0.005 UO_2^{2+} was obtained, by pH adjustment (pH =5), with dilute aqueous acid addition. The pH-meter used was a Voltcraft PH-100 ATC. The resulting synthesis mixture was stirred at 45°C for 7.5 h, and then heated at 80°C under static conditions for 15 h. The as-synthesized SBA-15 silica was recovered by filtration, washed with distilled water, dried and calcined at 550°C for 6 h (1°C min^{-1}).

Direct template exchange (sample D)

In this method, a 0.005 M uranyl nitrate precursor solution was adjusted to a pH of 5.0 and altered with surfactant cations into the as-synthesized SBA-15 silica for a period of 12 h, using a procedure described elsewhere [15, 27]. After being dried at 70°C, the sample was then calcined at 550°C for 6 h and exposed to air, and was designated sample D.C.

The uranyl-incorporated SBA-15 (sample I)

This sample was prepared using a calcined (800°C) SBA-15 support impregnated with a 0.005 M uranyl nitrate precursor solution adjusted to a pH value of 5.0 with a diluted solution of HNO_3.

2.3. Characterization methods

The structure and physicochemical properties of the materials were studied by means of a complex investigation system: X-ray diffraction (XRD), SEM/EDX (Energy dispersive X-Ray composition analysis), spectroscopic analysis via Fourier transform infrared spectroscopy (FTIR) and diffuse reflectance ultraviolet–visible spectroscopy (DRUV–VIS), and nitrogen adsorption/desorption at 77 K.

The powder X-ray diffraction patterns were collected on a TUR M-62 diffractometer under the following conditions: Ni filtered radiation Cu K_α = 0.1518 Å, a voltage of 36 kV, a current of 20 mA, and a goniometer speed of 0.5°/min. The a_0 parameter, calculated using the following formula, $a_0 = 2d_{100}/\sqrt{3}$, where d is the interplanar spacing, used for defining wall thickness (t) in the following relation: $t = a_0$ (the BJH pore diameter).

To determine the sample particle size and morphology, SEM images recorded on a VEGA TESCAN instrument, operating at an accelerating voltage of 20 kV. The determination of the chemical composition was performed on a Quantax system (Bruker AXS Microanalysis GmbH, Germany).

Porosity and surface area studies were performed on a NOVA 2200e system using nitrogen as the absorbate at liquid nitrogen temperature (-196°C). All the samples were out gassed under vacuum, for 6 hours at 25°C, before any adsorption measurements were made.

A FT-IR BRUKER ALPHA spectrometer was used to record infrared spectra of mesoporous materials in the region of 400-4000 cm^{-1}. DRUV-vis spectra were obtained at room temperature on a UV-vis spectrophotometer (Shimadzu UV-2401) in the wavelength range of 200-800 nm.

Dye model

The dye model of Eosin Y, a tetra-bromo derivate of fluorescein (IUPAC name: 2-(2,4,5,7-tetrabromo-6-oxido-3-oxo-3*H*-xanthen-9-yl) benzoate (CAS number 17372-87-1) was used. The structural formula of Eosin Y is shown in Scheme 1.

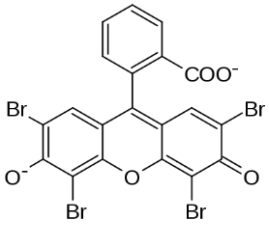

Scheme 1. The structural formula of Eosin Y

Eosin Y was purchased from Edward Gurr Ltd. All aqueous solutions were prepared using deionized water.

Photocatalytic degradation experiment

For each experiment, the reaction suspension was prepared by adding 0.075 g of the catalyst to 150 mL of the Eosin Y solution with an initial concentration of 10 mg/L. The suspension was stirred magnetically at 50 rpm, for 30 minutes in the dark to ensure absorption/desorption equilibrium between the dye molecules and the photocatalyst surface. Afterwards, the suspension was irradiated using a UV lamp. The UV-light source for the photocatalytic experiments was a 1000 Watt high-pressure mercury arc lamp (Oriel). During the photo degradation process, the UV lamp was positioned horizontally above the surface of the suspension. In all of the experiments, the reaction temperature was kept at 25 ±2ºC. Before the measuring the adsorption rates, at the predetermined time, samples of the examined solutions were centrifuged (20 min at 5000 rpm) to remove the solid catalyst. The upper clear liquid obtained after centrifugal separation was analyzed by UV-vis spectroscopy on a Shimadzu UV-2401 UV-Vis spectrophotometer. The maximum absorbance of the Eosin Y was found to be 516 nm, and the concentration of the solutions has been determined using the calibration curve. The degradation efficiency, as a function of the reaction time, was calculated considering the concentration ratio of the original solution and those of the analyzed samples (Eq.1).

$$\eta = (C_0\text{-}C) \cdot 100/C_0 = (A_0\text{-}A) \cdot 100/A_0 \quad (1)$$

where C_0 and A_0 are the initial concentration and absorbance of the Eosin Y solution at a fixed wavelength, corresponding to the maximum absorption wavelength; C and A are the concentration and absorbance of the Eosin Y solution after UV light irradiation at different time intervals, respectively.

3. Results and discussion

3.1. Morphological characterization

Some SEM images of uranyl modified SBA-15 samples are shown in Fig. 1. The siliceous matrix beams underwent morphological changes during treatment to obtain the uranyl/silica nanocomposites. Thus, there was a difference between the treatments based on ion exchange, in which the beams had dimensions similar to those of the matrix (large fibrous structures of 20–50 μm) and the hydrothermal treatment that was more aggressive, leading to a process of delamination, with smaller diameters (10–20 μm in diameter). Uranyl agglomerates could be observed on the surface, as shown in Fig. 1. Compared to the SEM images of the support (not shown here), it was noted that the fibrous surface was covered with deposits of uranium oxide.

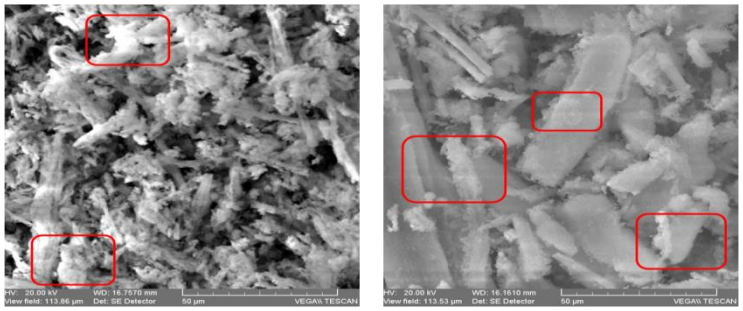

Fig. 1. Typical SEM –images of the studied samples: sample H (left) and sample I (right)

The siliceous fascicles belonging to the delaminated matrix were noticeable under hydrothermal synthesis conditions (Fig. 1, sample H; 10–20 μm in diameter). In contrast, sample I showed large fibrous structures of 20–50 μm, obtained by more gentle conditions (Fig. 2a; sample D).

The accumulated uranium concentration or weight percentage, i.e. At (atomic percentage) the for synthesized samples was determined using a Quantax apparatus (Bruker AXS Microanalysis GmbH, Germany); the results are presented in Table 1. The value varied between 2.737 and 3.476 wt%, depending on the method used.

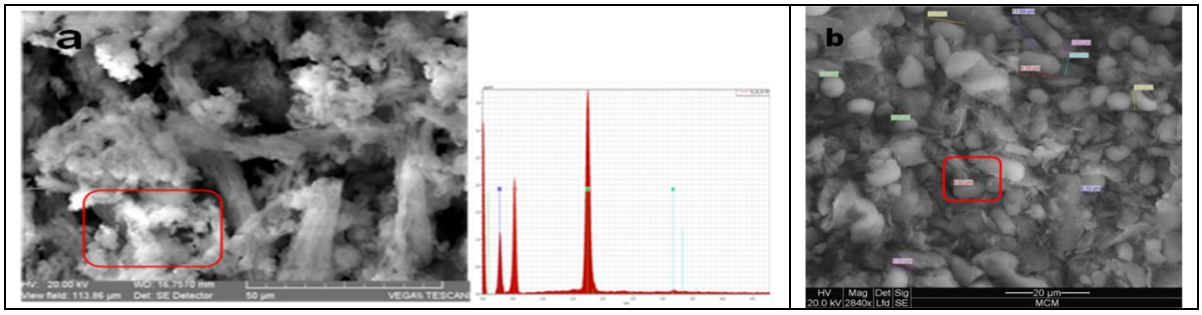

Fig. 2. SEM images: (a) and surface composition from EDX measurements/Wt: weight percent, At: atomic percent of D sample; (b) C sample

3.2. XRD results

The XRD diffractogram of the silica SBA-15 support (Fig. 3) shows well-resolved diffraction peaks at 2θ values of 1.07°, 1.77°, and 2.05°, which are a very good match to the (100), (110) and (200) Bragg reflections characteristic of this type of mesoporous silica having hexagonal (*P6mm*) 2D structure, in good agreement with reference data for mesoporous silica materials [15]. The XRD patterns (Fig. 3) suggest that the modification methods adopted to change the manner in which the uranium was incorporated led to a change in uranyl oxide encapsulation. The XRD patterns of uranyl-modified SBA-15 samples exhibited the same reflections characteristic of the hexagonal SBA-15 structure, indicating that the integrity of the parent structure was maintained after treatment. The d-spacing values calculated using the following formula $2d \sin\theta = n\lambda$ were also in the mesoporous range, but it was interesting to note that in the case of uranyl-modified SBA-15, the d_{100} spacing values increased compared to the support SBA-15 (Table 1). This indicates the presence of uranyl ions in the mesopores, in agreement with the published results [15]. The structural data are compiled in Table 1.

The XRD diffractograms of the studied samples in a smaller 2θ region are plotted below (Fig. 3).

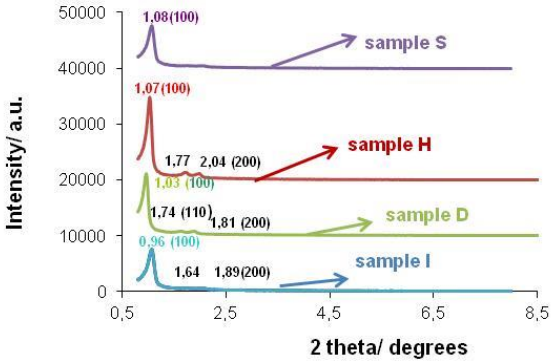

Fig 3. XRD pattern for samples S, H, D, I, at small, 2θ/degrees

In the XRD diffractograms of the uranyl-modified SBA-15 samples, in a higher 2θ region (Fig. 3), weak reflections appeared at 21.45-21.47°, 22.64°, 23.02°, 42.44°, 42.50-42.57°, 49.07-49.12° (Fig. 4), and 72.43° (Fig. 4), indicating the presence of ά-U_3O_8 moieties incorporated in the silica support, in accordance with the literature [10]. It worth noting that, when compared samples H, I and D, these reflections became more clear for sample I, in the order H>D>I, which is in accordance with the SEM images taken together, these results indicate that there was a greater accumulation of uranium in sample I. From sample I to H, the peak intensity specific to the (100) diffraction plane increased from 0.96 to 1.07, which was the highest value of all the studied samples.

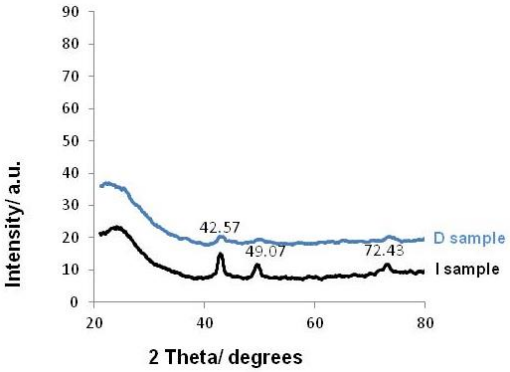

Fig. 4. XRD diffractograms belonging to D and I samples, at higher 2 Theta degrees

The mean crystallite sizes of the particles were calculated using the Scherrer equation (1), where D is the size of the particle, λ is the X-ray wavelength of incident X-rays (λ_{Cu} = 0.1541 nm), β is the full width at half-maximum intensity of the (100) peak, measured in radians, k is a constant (k=0.89), and θ is the diffraction peak of the (100) plane.

$$D = \frac{K \cdot \lambda}{\beta \cdot \cos\theta} \qquad (2)$$

Table 1. Parameters belonging to elemental cells and crystallite sizes for the envisaged samples

Sample	Accumulated Uranium concentration, wt %	2 θ	d_{100}	$a_{o,}$ nm	t^{*}/Δ^{**} (nm)	crystallite sizes
Sample S (SBA-15 sample)	-	1.07 (100) 1.77 (110), 2.05 (200)	85.20	9.77	4.20/0.62	3.8924
Calcinated H	3.476	1.07 1.77 2.04	89.92	9.77	4.20/0.00	3.8924
Sample D	2.998	1.03 1.72 1.8-1.97	91.45	9.83	5.28/1.08	1.977
Sample I	2.737	0.96 1.66 1.83	95.35	11.01	4.36/0.16	2.6498

$^{*}t = a_0$ (BJH pore diameter; see Table 2)
$^{**}\Delta$ - extra increase in wall thickness

In the case of sample I obtained by the impregnation method (C), the thickness of the pore walls (extra increase) was reduced in comparison with sample D (Method B), showing that the incorporation of uranium occurred within the pores. As far as sample H is concerned, this parameter remained unchanged. There are two aspects here that need pointing out, namely that the accumulated uranium concentration was highest in sample H, as well as the extra increase, leading to the idea that uranium/uranyl is incorporated within the siliceous fibers (extrapores). At higher 2θ values, weak reflections appeared at d = 4.15, 3.39, 2.62, 2.07, 1.96, and 1.75 Å, indicating the presence of α-U_3O_8 moieties encapsulated in the mesopores of the silica matrix.

Table 2 Structural parameters of the studied samples

Sample	Accumulated Uranium concentration, wt %	2 θ	d_{100}	$a_{o,}$ nm	t^{*}/Δ^{**} (nm)	crystallite sizes
Sample S (SBA-15 sample)	-	1.07 (100) 1.77 (110), 2.05 (200)	85.20	9.77	4.20/0.62	3.8924
Calcinated H	3.476	1.07 1.77 2.04	89.92	9.77	4.20/0.00	3.8924
Sample D	2.998	1.03 1.72 1.8-1.97	91.45	9.83	5.28/1.08	1.977
Sample I	2.737	0.96 1.66 1.83	95.35	11.01	4.36/0.16	2.6498

3. Characterization of the adsorptive attributes of the samples using the BJH Method

Pore sizes distributions were calculated from the desorption branches of the N2 adsorption isotherms using the Barrett-Joyner-Halenda (BJH) model.

3.4. BET results

The surface area was calculated using the BET method in the relative pressure range of 0.05-0.35. Pore volume was calculated at the relative pressure of 0.95. Fig. 5 shows nitrogen

adsorption-desorption isotherms for the materials. All samples displayed a typical type IV isotherm with an H1 hysteresis loop, which is characteristic of mesoporous materials, according to the IUPAC classification [27, 28].

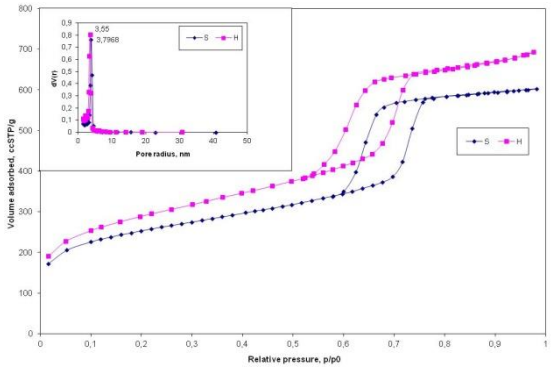

Fig. 5. N_2 adsorption/desorption isotherm and pore size distribution (the inset picture) of samples S and H

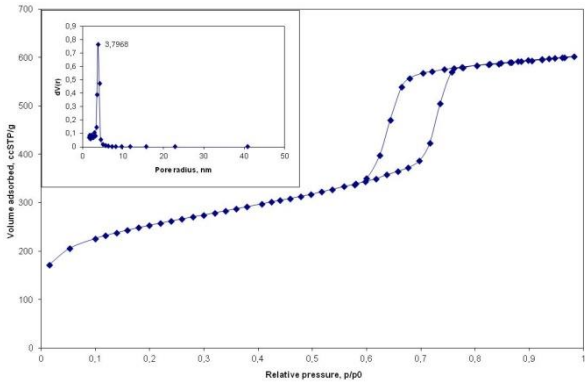

Fig. 6. N_2 adsorption/desorption isotherm and pore size distribution (the inset picture) of sample S

The hysteresis loops have sharp adsorption and desorption branches, indicating a narrow mesopore size distribution and the good quality of the samples. The observed decrease in surface area, pore diameter and pore volume provides evidence that the nanoparticles were located inside the pores (see Fig. 6). The reductions in surface area, pore volume, and pore diameter were due to the assimilation of uranyl species in the pores of the silica SBA-15 support, which caused a contraction of the nanopores by bridge-bonding of the uranyl species with silanol groups, as Fig. 7 revealed [13].

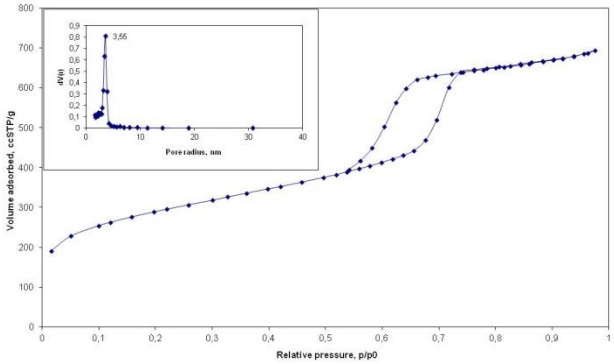

Fig. 7. N_2 adsorption/desorption isotherm and pore size distribution (the inset picture) of sample H

Figure 8 is a synthesis of Figs 5-7, in order to offer an overview of mesoporous profile of the envisaged materials.

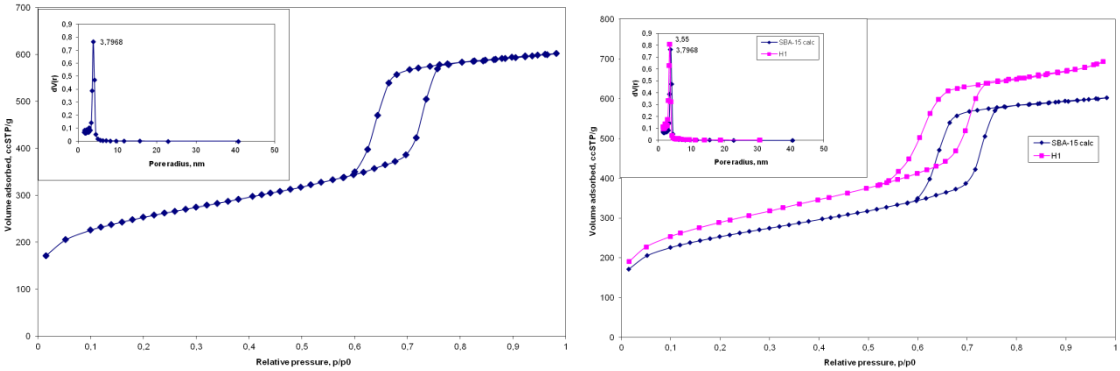

Fig. 8. N_2 adsorption/desorption isotherm and pore size distribution (the inset picture) of sample S (left) and samples H and I (right)

The structural attributes of studied samples are presented in the Table 3.

Tabel 3 Structural properties of studied samples

Sample	Pore diameter, nm	Surface area, BET, m^2/g	Pore volume, cm^3/g
S	7.15	749.5	1.421
H	5.3	644.377	0.884
D	4.9	517.509	0.752

3.5. FT-IR results

In the as-synthesized samples, the bands between 3200–3600 cm-1 correspond to νO–H vibrations and those at around 2920 and 2848 cm-1 correspond to the nC–H vibrations belonging to the organic compound [19, 20]. The bands around 1230 and 1060 cm-1 are due to -(Si–O–Si)- asymmetric stretching, na(Si–O–Si), whereas the bands at 794, 725, and 590 cm-1 are due to BSi–O–SiB symmetric stretching, ns(Si–O–Si). The band at 459 cm-1 may be linked to BSi–O–SiB bending (δSi–O–Si) vibrations.

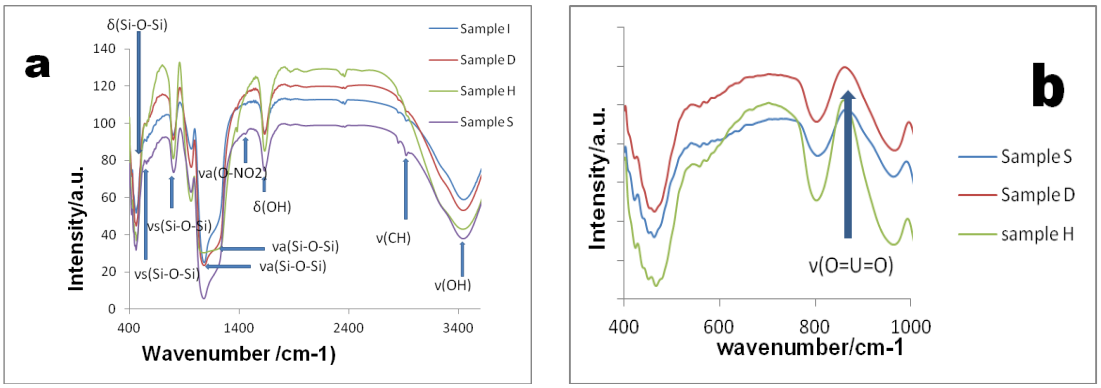

Fig. 9. FT-IR spectra of: a) uranyl incorporated SBA-15 samples by different synthesis routes; b) calcined samples in an enlarged wavenumber region (cm^{-1})

The bands in the range of 1700–1300 cm^{-1} are due to δ_{O-H}. All these bands are characteristic of a mesoporous silicate framework [20] (see Figs. 9a and 9b). In the case of the uranyl exchanged sample (D), the bands at around 1481, 1390, and 727 cm^{-1} are due to $\nu_a(O–NO_2)$, ν_a (NO_2), and $\delta(NO_2)$ vibrations, respectively [19], as seen in Figs. 7b and 9b. In addition, the IR band at 914 cm^{-1}, as seen in Fig. 9b, corresponds to the asymmetric stretching vibration, na(U=O), of the axial O=U=O group [20]. The frequency of this band was found to decrease progressively (Sample S>Sample D>Sample I)) with the change of synthesis route, as seen in the Fig 9. A modification in the ν_a(U=O), in terms of band width, from sample S (greater width) to sample D (uranyl exchanged SBA-15), was noted.

A downside of this study can be stressed, namely the very low concentration of uranyl entrapped in the silica matrix, a fact highlighted by the FT-IR analyses. Nevertheless, even at low concentrations, the results of photocatalytic experiments generated to very reliable results, namely eosin degradation. Consequently, further research will be conducted in order to progressively increase the uranyl concentration, aiming at optimizing the photocatalytic results.

3.6 UV-vis results

Between 450 and 600 nm broad transitions, otherwise not shown, are revealed by the the emission spectrum. In terms of DRUV–vis spectrum, broad bands centered at 254 and 425 nm with shoulders at 325 and 475 nm are associated to the uranyl sample (Fig. 10). The binding of the uranyl species with the host matrix in the equatorial plane of O=U=O, preserving the linearity of the axial bond, is very well sustained and endowed by the occurrence of overlapped, broad absorption and emission bands, compared to the well-defined, sharp transitions of the standard uranyl salt, due to electron-vibration interactions within the 350–500 nm region [3, 4, 17, 29]. Subsequently, one of the most relevant outcome of this study highlighted by DRUV–visible measurement reveal that the uranyl ions incorporated into SBA-15 retained their linear symmetry, similar to that in an aqueous solution. The adsorption spectra of uranyl supported on SBA-15 are usually shifted to lower values (at around 360 nm) due to the well-known quantum size effect [26]. Technically, this phenomenon is observable in the case of very small particle sizes (< 5 nm) [10].

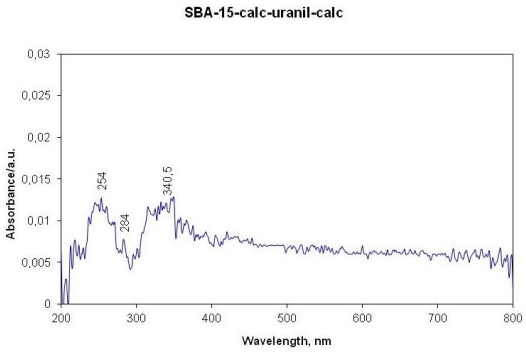

Fig. 10. DRUV–visible spectrum of the uranyl sample (SBA-15-calc-uranyl-calc)

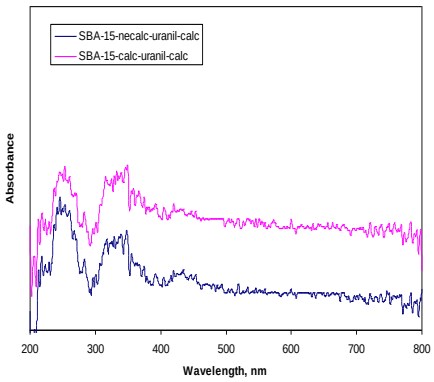

Fig. 11. DRUV–visible spectrum of the uranyl samples: SBA-15-calc-uranyl-calc; SBA-15-non-calc-uranyl-calc

Curve (a) in Fig. 10 shows the DRUV-VIS spectrum of the UO22 /SBA-15 sample. As in the case of Fig. 10, the DRUV-vis spectrum of the uranyl-anchored SBA-15 is comprised of broad and overlapping bands instead of sharp bands in the uranyl nitrate spectrum, which arose due to definite transitions from electronic levels coupled with O=U=O vibrations [30]. This may be attributed to the bonding of Si–O units and linear O=U=O molecules in the equatorial plane, forming an uranate type of local structure [9, 10]. The FT-IR study similarly provided evidence for the strong binding of the uranyl group, $(O=U=O)^{2+}$ with the BSi–O sites of the SBA-15 matrix [

8]. According to the stability requirement of a coordination structure, the uranyl groups can be envisaged as being anchored to the silicate matrix.

3.7 Photocatalytic results

To demonstrate the potential applicability of the uranyl-modified SBA-15 samples, the photocatalytic activity of these catalysts was evaluated by measuring the degradation of Eosin Y in water under ultraviolet illumination (Fig. 11).

Among all the specimens, sample I provided the best photocatalytic results Fig. 12 shows the spectra of residual Eosin Y after its degradation in terms of time elapsed.

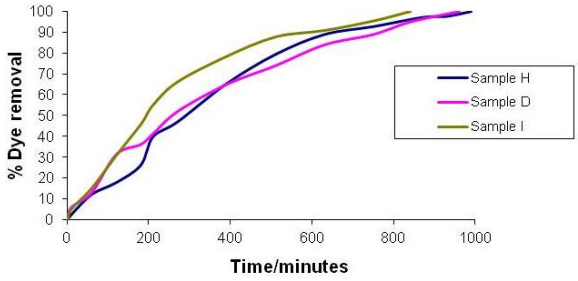

Fig. 12. Dye removal as a function of irradiation time

The outcome of this experiment correlated very well with both the XRD results and SEM images, supporting the idea that the best means of uranyl-incorporated SBA-15 synthesis is the impregnation method, namely sample I.

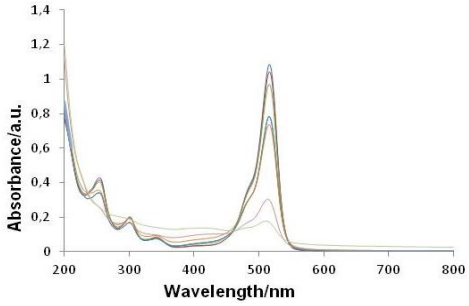

Fig. 13. Spectra of the remaining Eosin Y after photocatalytic degradation, as a function of irradiation time for: (a) sample H, (b) sample I, and (c) sample D

4. Conclusions

The observed decrease in surface area, pore diameter and pore volume provides evidence that uranyl nanoparticles were located inside the pores. The uranyl ions anchored to the mesopores of silica host matrices served as a highly efficient heterogeneous photocatalyst for the room-temperature photooxidation of Eosin Y. The results show the potential applicability of uranyl anchored to the SBA-15 silica photocatalyst for applications related to wastewater processing under ambient conditions.

Acknowledgements

Scientific research financed from "Grigore T. Popa" University of Medicine and Pharmacy of Iasi, according to the 31589/23.12.2015 research contract. The authors are also acknowledged „Lucian Blaga" University of Sibiu research grants LBUS-IRG-2015-01.

References

[1] M.J. Keith-Roach, (2008), Sci Total Environ. 396 (2008).
[2] C.D. Klaassen, Casarett and Doull's Toxicology, McGraw-Hill Press, New York (2008).
[3] J.C. Seaman, T. Meehan, P.M. Bertsch, J Environm. Qual. **30**, 1206 (2001).
[4] C.J. Chisthom-Brause, J.M. Berg, R.A. Matzner, D.E. Morris, J Coloid Interf. Sci. **233**(1) (2001).
[5] D. Humelnicu, E. Popovici, E. Dvininov, C. Mita, J Radioanal. Nucl. Chem. **279**(1) (2009)
[6] J. Dent, J.D.F. Ramsay, S.W. Swaanton, J Colloid Interf. Sci, 150 (1992)
P. Michard, E. Guibal, T. Vincent, P. Cloirec, (1996), Micropor. Mater, 5 (1996).
[7] S. Aytas, S. Akyil, M.A.A. Aslani, U. Aytekin, J Radioannal. Nucl .Chem **240**, 973 (1999).
[8] A.R. Gupta, B. Venkataramani B. Chem. Soc. Jpn. **61**, 1357 (1988).
K. Vidya, S.E. Dapurkar, P. Selvam, S.K. Badamali, N.M. Gupta, Micropor. Mesopor. Mater. (2001).
[9] J.S. Beck, J.C. Vartuli, W.J. Roth, M.E. Leonowicz, K.D. Schmidtt, C.T.-W Chu, D.H. Olson, E.W. Sheppard, S. McCullen, J.B. Higgins, J.L. Schlenker, J Am. Chem .Soc. **114**, 10834 (1992).
[10] P. Selvam, S.K. Bhatia, C. Sonwane, Ind. Eng. Chem. Res. **40**, 3237 (2001).
[11] X. Wang, K.S. Lin, J.C. Chan, S. Cheng, J Phys .Chem. B. **109**(5) (2005).
[12] K. Vidya, V.S. Kamble, N.M. Gupta, P. Selvam, Studies Surf. Sci.Catal, 156 (2005).
[13] K. Vidya, V.S. Kamble, P. Selvam, N.M. Gupta, Appl Catal B: Environ. **54** (3) (2003).
[1] Y.S. Shin, M.C. Burleigh, S. Dai, C.E. Barnes, Z.L. Xue, Radiochim. Acta **84**, 37 (1999).
[14] K. Vidya, S.E. Dapurkar, P. Selvam, S.K. Badamali, D. Kumar, N.M. Gupta, J Mol. Catal A: Chem. 181 (2002).
[15] D. Kumar, S. Bera, A.K. Tripathi, G.K. Dey, N.M. Gupta, Micropor. Mesopor. Mater. (2003).
[16] D. Kumar, V.S. Kamble, N.M. Gupta, Catal. Lett, 88 (2003).
[1] E. Rabinowitch, R.L. Belford, Spectroscopy and Photochemistry of Uranyl Compounds, Pergamon Press, Oxford (1964).
[17] V. Balzani, F. Bolletta, M.T. Gandolfi, M. Maestri, Top. Curr. Chem. **8**(75) (1997).
[18] H.D. Burrows, T.J. Kemp, Chem. Soc. Rev. 3 (1974)
[19] S.L. Suib, A. Kostapapus, D.J. Psaras, J Am. Chem. Soc. **106**, 1614 (1984).
[20] S.L. Suib, K.A. Carrado, Inorg. Chem. **24**, 863 (1985).
[21] S.L. Suib, J.F. Tanguay, M.L. Occelli, J Am. Chem. Soc. 108 (1986).
[22] D. Zhao, J. Feng, Q. Huo, N. Melosh, G.H. Fredrickson, B.F. Chmelka, G.D. Stucky, Sci. 279 (2009).
[23] K. Vidya, Mat. Res. Bull., 39 (2004).
[24] IUPAC Pure Appl. Chem, **66**, 1739 (1994)
[25] K. Vidya, V.S. Kamble, N.M. Gupta, P. Selvama, J. Catalysis **247**, 1 (2007).
[26] S. Olmez, S. Aytas, M. Akyil, J. Eral, J Radioannal. Nucl. Chem, **260**(1) (2004).